

Observation and Modeling of the circular polarization of the Cr I magnetic field induced transition at 533.03 nm

HAO LI,^{1,2} TANAUSÚ DEL PINO ALEMÁN,^{1,2} JAVIER TRUJILLO BUENO,^{1,2,3} AND FRANZISKA ZEUNER⁴

¹*Instituto de Astrofísica de Canarias, E-38205 La Laguna, Tenerife, Spain*

²*Departamento de Astrofísica, Universidad de La Laguna, E-38206 La Laguna, Tenerife, Spain*

³*Consejo Superior de Investigaciones Científicas, Spain*

⁴*Istituto ricerche solari Aldo e Cele Daccò (IRSOL), Faculty of Informatics, Università della Svizzera italiana, CH-6605 Locarno, Switzerland*

ABSTRACT

We study the circular polarization of the magnetic field induced transition (MIT) between the $3d^5(6S)4d\ ^7D_2$ and $3d^5(6S)4p\ ^7P_4^\circ$ states of Cr I at 533.03 nm (wavelength in air). The fractional circular polarization V/I of this spectral line resulting from the solution of the radiation transfer problem in a sunspot model permeated by a homogeneous magnetic field of 3 kG shows amplitudes of about 2%. Spectro-polarimetric observations of two sunspots were obtained with the Zurich Imaging Polarimeter-3 at the Istituto ricerche solari Aldo e Cele Daccò (IRSOL) observatory in Locarno, Switzerland. The observed V/I profiles show approximately anti-symmetrical shapes with an amplitude of around 0.1% and 0.2% for the two sunspots. The center of this profile coincides with the wavelengths predicted for the above-mentioned MIT. We apply an inversion code to the spectro-polarimetric data of the Cr I permitted lines at 532.91 and 532.98 nm, as well as to the MIT line at 533.03 nm, to infer a stratification of the emitting atmosphere. We compare the V/I profiles synthesized in the inferred atmosphere models with the observations, showing that the observed signal likely corresponds to the MIT line.

1. INTRODUCTION

Magnetic field induced transitions (MIT) are forbidden transitions, i.e., not fulfilling the relevant selection rules, whose oscillator strength is enhanced due to the state-mixing induced by the presence of a magnetic field, as the quantum number that made them forbidden ceases being a good quantum number. Beiersdorfer et al. (2003) identified a MIT of Ar IX in a laboratory experiment for magnetic fields in excess of 10 kG. Relatively recently, theoretical investigations were carried out by Li et al. (2013) and Grumer et al. (2014) to accurately compute the transition rates of MITs.

During the last years there has been a growing interest of the MITs in solar physics research, in particular in relation to magnetic field inference in the solar corona. Since the transition rate of a MIT depends on the degree of mixing of atomic states, this rate is therefore sensitive to the magnetic field strength. In particular, the Fe X MIT at 257.26 Å has been proposed as a probe of the magnetic field in the solar corona (Li et al. 2015, 2016, 2021, and Judge et al. 2016). A laboratory experiment by Xu et al. (2022) has demonstrated the potential of this line for magnetic field diagnostics.

The Fe X MIT at 257.26 Å has been used to infer the coronal magnetic field strength in active regions (Si et al. 2020; Landi et al. 2020, 2021, and Brooks et al. 2021) from observations obtained by the EUV Imaging Spectrometer onboard the Hinode satellite (Culhane et al. 2007). Chen et al. (2021a,b, 2023a); Martínez-Sykora et al. (2022), and Liu et al. (2022) have also demonstrated, using magneto-hydrodynamic models, that the Fe X MIT line can be used to determine the magnetic field strength not only in the solar corona, but also in the corona of other stars. For a review of both the theory to compute the transition rates of MIT and the application of the magnetic inference method to the solar corona, see Chen et al. (2023b).

The above-mentioned investigations focused on the intensity of the considered MIT. In order to study the polarization of a MIT, and motivated by the fact that the Sun is a laboratory for atomic physics research, we have checked the solar visible spectrum in the search of a MIT, of which the polarization can be observed from ground based solar telescopes. The transition rate of a MIT, to the first-order perturbation approximation, is proportional to $B^2\lambda^{-3}\Delta E^{-2}$ (Li et al. 2015), with B the magnetic field strength, λ the wavelength of the transition, and ΔE the energy separation between the mixed

states. Therefore, the smaller the energy separation between mixing states, the larger the transition rate of the MIT.

In this work we report on the Cr I MIT at 533.03 nm, pertaining to the multiplet with upper term $3d^5(^6S)4d^7D$ and lower term $3d^5(^6S)4p^7P^\circ$. The fine structure separation within the upper term is on the order of 10^{-4} eV. Due to its relatively small ionization potential, the Cr I atoms are dominant mainly in the relatively cold photosphere, where the magnetic field is typically stronger compared with the upper layers of the solar atmosphere. Another advantage of this line is that it is spectrally resolvable, i.e., it is not blended with permitted lines of the same multiplet (as it is the case for the already mentioned Fe X 257.262 Å or Ar IX lines), due to its relatively long wavelength. Furthermore, the Zeeman split of this transition is significant. For all these reasons, the circular polarization of this MIT can be observed in sunspots from ground-based telescopes.

In Section 2 of this paper we briefly introduce the atomic model used in the radiative transfer (RT) modeling of the Cr I MIT. The line profiles synthesized in model C of Fontenla et al. (1993; hereafter, FALC model) and model E of Maltby et al. (1986; hereafter, M-E model) are compared with the solar spectral atlas. In Section 3 we show the observations in two sunspots acquired with the Zurich Imaging Polarimeter-3 (ZIMPOL-3; Ramelli et al. 2010) at the IRSOL located in Locarno, Switzerland. We apply the HanleRT Tenerife Inversion Code (HanleRT-TIC; del Pino Alemán et al. 2016; Li et al. 2022) to invert the data and infer the stratification of the underlying solar atmosphere. The fractional circular polarization V/I profiles of the Cr I MIT synthesized in the inferred model atmosphere are shown and compared with the observation. Our conclusions are summarized in Section 4.

2. ATOMIC MODEL AND SPECTRAL SYNTHESIS

The upper (${}^7D_{1,2,3,4,5}$) and lower (${}^7P_{2,3,4}^\circ$) terms of the Cr I MIT at 533.03 nm, as well as the ground level of Cr I, are shown in the Grotrian diagram in Fig. 1. There are nine electric dipole (E1) transitions between the two terms, indicated by the solid line arrows. The six transitions indicated by the dashed line arrows are induced due to the atomic state-mixing in the presence of external magnetic fields, i.e. they are the MITs. The corresponding wavelengths are 527.38, 527.46, 529.66, 529.88, 533.03, and 533.06 nm, respectively. The energy separations of the fine structure levels of the upper term 7D are on the order of 10^{-4} eV. The small energy separation allows for a significant degree of state-mixing.

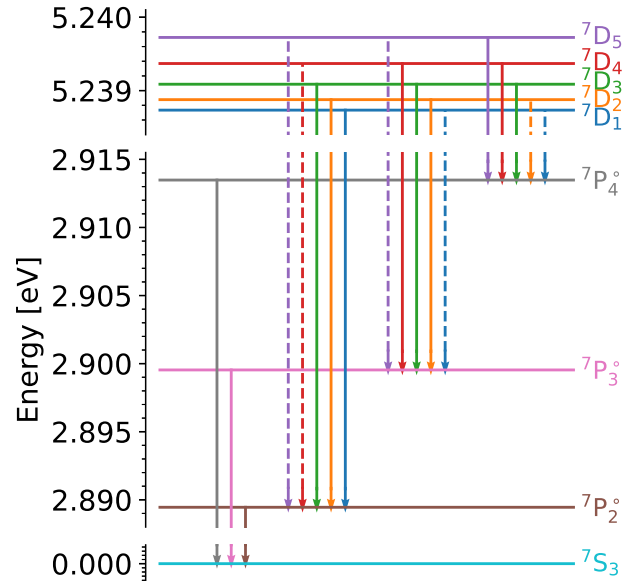


Figure 1. Grotrian diagram showing the Cr I $3d^5(^6S)4s^7S$, $3d^5(^6S)4p^7P^\circ$, and $3d^5(^6S)4d^7D$ terms. The energy values are taken from the NIST database (Kramida et al. 2022). The solid line arrows indicate the E1 transitions, while the dashed line arrows indicate the MITs.

Within the Russell-Saunders (LS) coupling scheme, the transition rate between two terms and the rate between two J levels are related by the following expressions (e.g., Landi Degl’Innocenti & Landolfi 2004),

$$A(L_u S J_u \rightarrow L_l S J_l) = (2L_u + 1)(2J_l + 1) \times \left\{ \begin{matrix} L_u & L_l & 1 \\ J_l & J_u & S \end{matrix} \right\}^2 A(L_u S \rightarrow L_l S), \quad (1a)$$

$$A(L_u S \rightarrow L_l S) = \sum_{J_\ell} A(L_u S J_u \rightarrow L_l S J_\ell), \quad (1b)$$

where L_u and L_l are the orbital angular momenta of the upper and lower terms, respectively, J_u and J_l are the total angular momenta of the upper and lower levels, respectively, and S is the spin angular momentum. $A(L_u S J_u \rightarrow L_l S J_l)$, and $A(L_u S \rightarrow L_l S)$ are the Einstein coefficients for emission, proportional to the transition rate, from the level $L_u S J_u$ to $L_l S J_l$, and from the term $L_u S$ to $L_l S$, respectively. In the multi-term approach, the quantum state coupling between the fine structure levels within a term (all the J levels for a given spin S and orbital angular momentum L) is taken into account, and the total angular momentum J is thus not a good quantum number. This coupling is instead neglected in the multi-level ap-

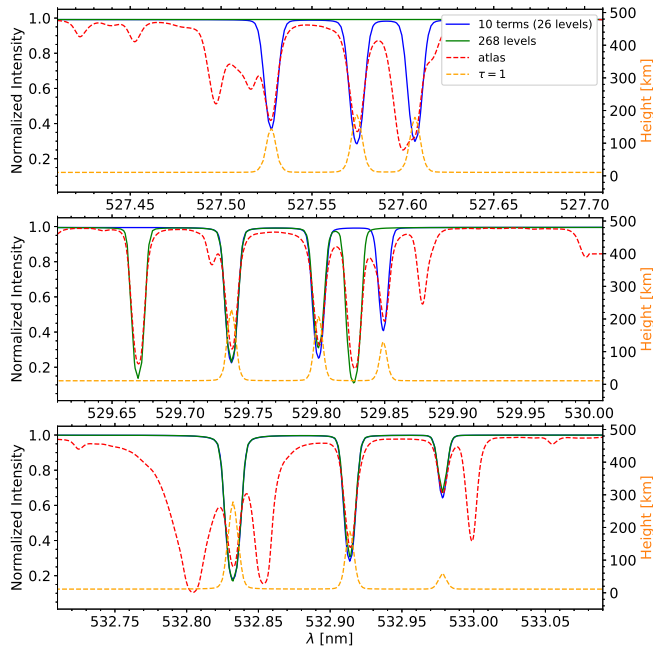


Figure 2. Intensity profiles at disk center resulting from the solution of the RT problem in the FAL-C model with a Cr multi-level model with 268 levels (green curve) and with a multi-term model with 26 atomic levels (blue curve). The red dashed curve shows the solar spectral atlas of the quiet Sun (Delbouille et al. 1973). The intensity profiles have been normalized to their value at the continuum. The orange dashed curves (see right axis) show the height where the optical depth is equal to one. The three panels show different spectral ranges, covering all spectral lines in the multiplet of interest.

proach (see §7 in Landi Degl’Innocenti & Landolfi 2004, for further details on multi-level and multi-term model atoms). While in theory the transition probability obtained from Eq. (1b) is expected to be the same for every J_u , they often differ in practice. It is thus necessary to estimate an average $A(L_u S \rightarrow L_\ell S)$ accounting for every J_u level. In previous works we have taken the average weighted by the degeneracy of the upper level (del Pino Alemán et al. 2020). However, due to the lack of data for some of the fine structure transitions in this multiplet, we have taken the average value among the available ones.

$$\bar{A}(L_u S \rightarrow L_\ell S) = \frac{1}{5} \sum_{J_u J_l} (2L_u + 1)^{-1} (2J_\ell + 1)^{-1} \times \begin{Bmatrix} L_u & L_l & 1 \\ J_l & J_u & S \end{Bmatrix}^{-2} A(L_u S J_u \rightarrow L_l S J_l), \quad (2)$$

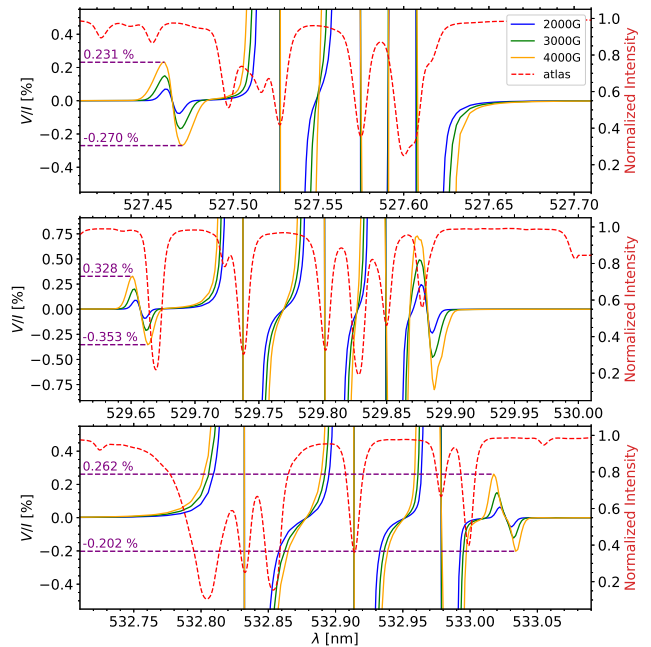


Figure 3. Fractional circular polarization V/I profiles at disk center resulting from the solution of the RT problem in the FAL-C model with a Cr multi-term model with 26 atomic levels, imposing an homogeneous magnetic field of 2 (blue curve), 3 (green curve), and 4 kG (orange curve). The red dashed curve (see right axis) shows the intensity in the solar spectral atlas of the quiet Sun (Delbouille et al. 1973). The three panels show different spectral ranges, covering all spectral lines in the multiplet of interest.

where the sum runs over the levels for which we have a value of the transition probability. The $L_u S J_u \rightarrow L_\ell S J_\ell$ transition probability which correspond, via Eq. (1a), to the derived $L_u S \rightarrow L_\ell S$ transition probability within the LS coupling scheme differ from the NIST ones by about a $\sim 5\%$, except for the $J_u = 3 \rightarrow J_l = 3$ transition, which differs by about $\sim 20\%$. In Table 1, we list the transition rates derived via Eq. (1a) and those from the NIST database. The energy level of the magnetic sub-levels and the MIT rates as a function of magnetic field strength are show in Appendix A. The magnetic quadrupole (M2) transition rates between the two terms of interest are on the order between 10^{-4} and $10^{-7} s^{-1}$, estimated with the multi-configuration Dirac-Hartree-Fock method (Li et al. 2020). These rates are too small to significantly contribute to the observable signal, and are therefore neglected.

The bound-bound collisional rates with electrons are estimated following van Regemorter (1962) for the E1 transitions, and following Bely & van Regemorter

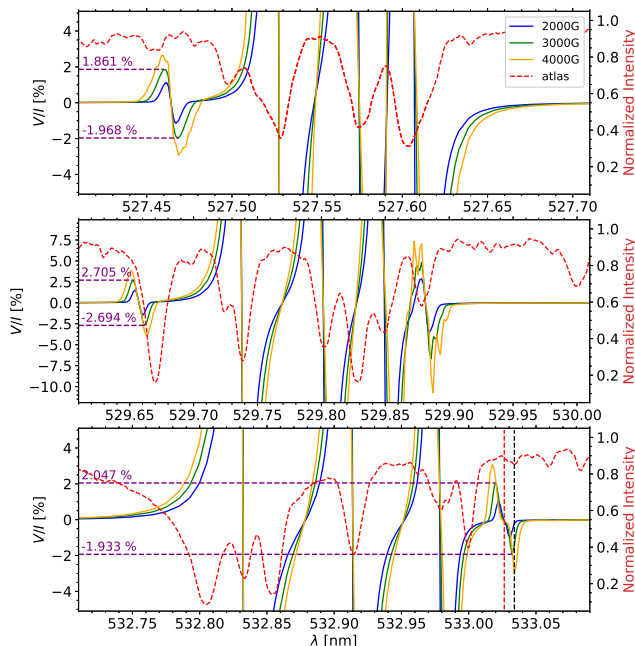


Figure 4. Same than Fig. 3, but for the M-E model and the sunspot atlas (Wallace et al. 2005). The vertical black dashed line indicates the center of the absorption feature close to 533.03 nm, while the vertical red dashed line indicates the zero crossing of the circular polarization profile of the nearby MIT.

Table 1. Wavelengths and transition rates of the nine E1 transitions, and the formation heights of the nine lines. A_{NIST} denotes the rate from NIST database, while A is rate obtained from Eq. (1a).

Transition	λ (air) (nm)	A_{NIST} (s^{-1})	A (s^{-1})	$\tau_{\lambda} = 1$ height (km)
${}^7D_3 \rightarrow {}^7P_2^{\circ}$	527.53	-	1.67e7	140
${}^7D_2 \rightarrow {}^7P_2^{\circ}$	527.57	-	3.90e7	190
${}^7D_1 \rightarrow {}^7P_2^{\circ}$	527.61	-	5.85e7	180
${}^7D_4 \rightarrow {}^7P_3^{\circ}$	529.74	3.88e7	3.65e7	230
${}^7D_3 \rightarrow {}^7P_3^{\circ}$	529.80	3.0e7	3.65e7	210
${}^7D_2 \rightarrow {}^7P_3^{\circ}$	529.85	-	1.95e7	130
${}^7D_5 \rightarrow {}^7P_4^{\circ}$	532.83	6.2e7	5.85e7	280
${}^7D_4 \rightarrow {}^7P_4^{\circ}$	532.91	2.25e7	2.20e7	190
${}^7D_3 \rightarrow {}^7P_4^{\circ}$	532.98	5.38e6	5.22e6	60

(1970) for the forbidden transitions. The bound-free collisional rates with electrons were estimated following Allen (1973). The photoionization cross sections are taken as hydrogenic (see, e.g., Mihalas 1978).

Since the ionization potential of Cr I is relatively low, we have some Cr II levels and the ground level of Cr III in our atomic model, as they impact the Cr I ionization fraction. We use the HanleRT code (del Pino Alemán et al. 2016, 2020) to solve the RT problem out of local thermodynamical equilibrium (non-LTE). Fig. 2 shows the intensity profiles synthesized in the FAL-C model. The wavelengths are converted from their values in vacuum to those in air by assuming that the refractive index of air is 1.00027825 at 530 nm (Ciddor 1996). The green curves in the figure show the profiles computed with a multi-level atomic model consisting of 143 Cr I levels, 122 Cr II levels, and the ground level of Cr III, while the blue curves show the profiles computed with a multi-term atomic model consisting of 6 (16) Cr I terms (levels), 3 (9) Cr II terms (levels), and the ground term of Cr III. The red dashed curves in the figure show the solar spectral atlas of the quiet Sun (Delbouille et al. 1973).¹

Clearly, the 268-level atomic model (green curves) is more accurate, as the corresponding synthesized profiles can fit the main features of the Cr lines in the atlas. The Cr absorption lines at 527.53, 527.57, 527.61, and 529.85 nm are missing due to the lack of transition rates in the NIST database. The blue curves show the profiles synthesized with a multi-term 10-term (26 levels) atomic model. The missing transition rates are “automatically filled” through the expressions for the transfer and relaxation rates, and the RT coefficients (see Eq. (1a) and §7.6 of Landi Degl’Innocenti & Landolfi 2004). The difference between the synthesis and the spectral atlas is not significant, which indicates that this reduced model atom is good enough for the purpose of this paper, significantly reducing the computational requirements. Hereafter, all the calculations are performed with the 10-term atomic model.

Finally, the orange curves in Fig. 2 indicate the height where the optical depth τ_{λ} is equal to one, which roughly indicates the formation heights. The corresponding heights at the line center are listed in Table 1. All the nine E1 lines form in the photosphere, with the line at 532.98 nm forming lower than the rest.

In the presence of external magnetic fields, six transitions are induced due to state-mixing. Fig. 3 shows the Stokes V/I profiles synthesized in the FAL-C model with longitudinal magnetic fields of 2000, 3000, and 4000 G, respectively, for a line of sight with $\mu = 1.0$, where μ is the cosine of the heliocentric angle. The V/I amplitudes of the four MITs are on the order of 10^{-3} . The

¹ https://bass2000.obspm.fr/solar_spect.php

other two MITs are not shown due to their weak signal. The amplitude of the line at 529.88 nm is larger than those of the other 3 lines, since the energy separation between 7D_1 and 7D_2 is smaller than others. Besides, it can be seen that the amplitudes of the two lobes of the MIT are not exactly the same. This is because the MIT rates between M states are not symmetric due to the different degrees of state-mixing for each M state (see Appendix A). The asymmetric nature of these transition rates can also be seen in Table 3 in Li et al. (2021), and are only significant for strong magnetic fields.

Figure 4 shows the synthesized profiles in the M-E model. In the sunspot model, the temperature is lower than in the FAL-C model. More Cr atoms are found in its neutral stage and the lines are narrower. Consequently, larger V/I amplitudes of around 2% in the MIT lines are present. The profiles at 527.46 nm and 529.88 nm are not smooth for a field strength of 4000 G, because the Zeeman splitting of such a strong magnetic field is comparable with the line width. The red dashed curves show the spectral atlas of a sunspot (Wallace et al. 2005).² In contrast to the atlas of the quiet sun, there is an additional weak absorption feature near 533.03 nm. The center of the absorption is denoted by the black dashed curve, and it does not coincide with the zero crossing of the circular polarization profile of the MIT (indicated with a red dashed line in the figure). This absorption feature could correspond with an unknown molecular line. Comparing with the atlas, we find that the two of the MIT lines at 529.65 and 529.87 nm are blended with strong lines. Contrarily, the lines at 527.46 and 533.03 nm are not too much contaminated. Especially, the line at 533.03 nm appears to blend solely with an unknown weak absorption feature, and it should be detectable with current solar telescopes and instrumentation.

3. OBSERVATION AND INVERSION

Spectro-polarimetric observations of the intensity and circular polarization of the Cr I lines around 533 nm in the NOAA AR 13102 and 13153 were acquired on 20 September and 6 December 2022, respectively. Both were located far from the solar limb. We employed the high-sensitivity ZIMPOL-3 spectropolarimeter (using the photo elastic modulator, as described in Ramelli et al. 2010) at the 45 cm aperture IRSOL Gregory Coudé Telescope in Locarno, Switzerland, alongside a Czerny-Turner spectrograph, incorporating an interference pre-filter. The spectral sampling is 7.5 mÅ.

The slit-jaw images are shown in the top left panels of Figs. 5 and 6, with the position of the slit indicated by the black line. Additionally, the slow modulation technique was used to enhance the zero-level accuracy of the circular polarization (Zeuner et al. 2022). The data are reduced with the standard reduction (dark image and flat field correction as well as polarimetric calibration) software but are not corrected for spatial or spectral stray light. The spectral stray light is on the order of 2%, mostly affecting the depth of the spectral lines. The core of the sunspot might be compromised by stray light contributions from the telescope, instruments, and the sky. As a result, the Stokes V/I profile amplitudes might be decreased. However, as we will show later, we are not interested in a detailed inversion of this region, as our argument is based on a consistent modeling of multiple Stokes V/I profiles. The intensity and fractional circular polarization profiles resulting from the spatial average over several arcsec along the spectrograph slit is shown in the top right and bottom row of Figs. 5 and 6, respectively. In the bottom right panel of these figures we show the fractional circular polarization V/I around the MIT. The red dashed line indicates the line center of the MIT, while the black dashed line indicates the line center of the absorption feature observed in the sunspot atlas. There is no evidence of any feature in the intensity profile that can be identified as the MIT. However, the fractional circular polarization profile shows an approximately anti-symmetric shape centered in the wavelength where the MIT is expected. The amplitude of this fractional circular polarization is about 0.1% in NOAA AR 13102 and 0.2% in NOAA AR 13153, clearly above the statistical noise level of 0.02% and 0.07% estimated by the RMS of the fractional circular polarization V/I profile in the continuum between the two blue vertical lines shown in the bottom left panel of Figs. 5 and 6.

We applied our non-LTE inversion code, HanleRT-TIC, to the observations of the Cr I permitted lines at 532.91 and 532.98 nm, and the MIT at 533.03 nm, assuming $\mu = 1.0$. The orange circles in Figs. 5 and 6 indicate the wavelengths included in the inversion. We considered a model atmosphere stratified in 60 nodes distributed between $\log_{10}(\tau_{500}) = -6.5$ and 1.5, and gave a larger weight (50 times larger than the E1 transitions) to the circular polarization of the MIT under investigation due to its weak signal. Two cycles are employed to invert the profiles. The gas pressure at the top boundary is fixed at 1 dyn/cm⁻². In the first cycle, we adopted 4 nodes in the field strength, 4 nodes in the inclination of the magnetic field, 5 nodes in the temperature, and 1 node in the vertical velocity. Note that we did not observe the linear polarization. The transverse

² <https://nispdata.nso.edu/ftp/pub/atlas/spot4at1/>

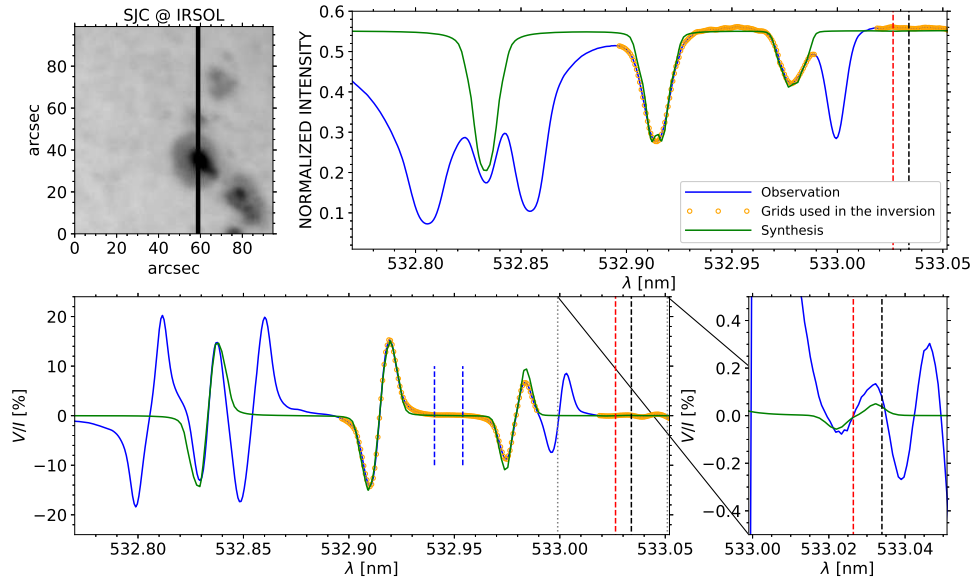


Figure 5. Slit-jaw image (top left), intensity profile (top right), and fractional circular polarization V/I profile (bottom row) for the NOAA AR 13102 observed on 20 September 2022 with the ZIMPOL-3 at the IRSOL observatory. The black line in the top left panel indicates the location of the spectrograph's slit. The blue solid curves show the profiles in the observation, the green solid curves show the profiles in the synthesis in the atmospheric model resulting from the inversion, and the orange open circles indicate the wavelengths included in the inversion. The red dashed line indicates the line center of the MIT and the black dashed line indicates the center of an absorption feature in the sunspot atlas. Finally, the dotted lines indicate the wavelength range plotted in the bottom right panel. The noise level is 0.023% estimated by the RMS of the fractional circular polarization V/I in the continuum between the two vertical blue dashed lines.

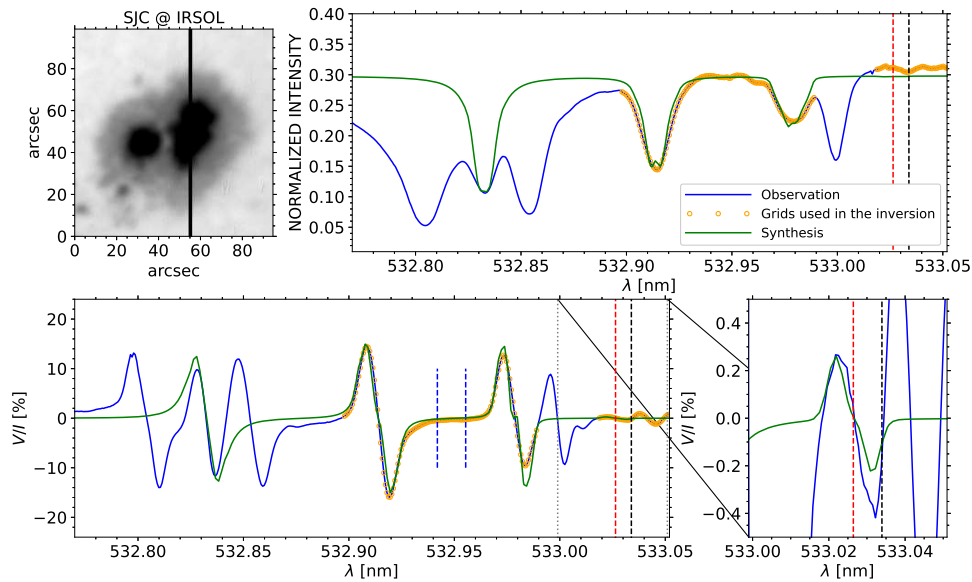


Figure 6. Same as Fig. 5, but for NOAA AR 13153 observed on 6 December 2022. The noise level is 0.068% estimated by the RMS of the V/I in the continuum between the two vertical blue dashed lines.

magnetic field is included as a source of line broadening. Besides it also contributes to the level mixing and furthermore impacts the MIT. In the second cycle, we adopted 4 nodes in the field strength, 4 nodes in the inclination of the magnetic field, 7 nodes in the temperature, 4 nodes in the vertical velocity, and 1 node in the micro-turbulent velocity to improve the fitting. The inverted longitudinal magnetic field in the lower photosphere of the inverted models is about -1000 G for NOAA AR 13102 and about 2000 G for NOAA AR 13153.

The green curve in Figs. 5 and 6 show the intensity and fractional circular polarization profiles synthesized in the inferred model atmosphere. The synthetic profiles reproduce the main features of the observation, even for the line at 532.83 nm despite it being neglected in the inversion. The fractional circular polarization amplitudes of the MIT are similar to those in the observed profiles. The main reason for the differences are likely due to the fact that the observed profiles are averages over several arcsec along the slit, mixing different parts of the sunspot, which cannot be represented in a single and relatively simple sunspot model. Nearby lines might also contaminate the profiles, especially the probably unknown molecular line indicated by the black dashed line in Fig. 4-6.

4. CONCLUSION

In this work we have identified a Cr I MIT at 533.03 nm. The upper term, $3d^5(^6S)4d^7D$, consists of 5 fine structure levels with an energy separation on the order of 10^{-4} eV, a relatively small energy which facilitates the J -state mixing in the presence of external magnetic fields with a strength that can be typically found in the solar photosphere of solar active regions. The solution of the non-LTE RT problem in semi-empirical models shows fractional circular polarization V/I amplitudes of about 0.1% in a quiet Sun model and about 1% in a sunspot model, when imposing a 3000 G longitudinal magnetic field in both cases. The amplitudes of the circular polarization lobes of the MIT are not exactly anti-symmetrical, due to the different degrees of state-mixing for each M state.

Spectro-polarimetric observations of two active regions were obtained with the ZIMPOL-3 at the IRSOL. While there is no feature in the intensity profile that can be identified with the Cr I MIT, the fractional circular polarization profiles show a clear approximately anti-symmetric shape whose center coincides with the wavelength predicted for the MIT. The amplitudes of the circular polarization profiles are about 0.1% and 0.2% in the two sunspots, well above the polarization noise

level estimated from the RMS of the fractional circular polarization V/I in the continuum.

Applying HanleRT-TIC, we performed non-LTE inversions on the profiles of three Cr I lines in the observation, including the MIT. We show the intensity and circular polarization profiles resulting from the solution of the non-LTE RT problem in the inferred model atmospheres. These synthetic profiles show fractional circular polarization amplitudes similar to those in the observations, with the discrepancies likely explained by the contamination of nearby lines (partial blends) and the spatial averaging of the data over several arcsec. All-in-all, the fractional circular polarization profiles observed at 533.03 nm, with no counterpart in the intensity profile, are very likely due to the predicted Cr I MIT.

While MIT lines such as the one studied in this paper are only detectable in the presence of magnetic fields above a certain strength, the potential for photospheric magnetic field diagnostic of these lines is extremely limited. While the mere presence of the MIT line is evidence of a magnetic field, the magnetic field strength that is usually required is so large that the magnetic field is already evident from several other observables (e.g., the sunspot itself). Moreover, due to the small strength expected for the MIT for the typical magnetic fields expected in the Sun, their signals are very susceptible even to partial blends with nearby spectral lines. Therefore, the usefulness of the MIT for the diagnosis of solar magnetic fields is likely limited to highly ionized species in the corona.

ACKNOWLEDGMENTS

We thank Michele Bianda for helpful technical assistance, Andrés Asensio Ramos for helpful comments and suggestions, and Wenxian Li for carefully reading the manuscript and providing us the M2 transition rates. We acknowledge the funding received from the European Research Council (ERC) under the European Union’s Horizon 2020 research and innovation programme (ERC Advanced Grant agreement No 742265). T.P.A.’s participation in the publication is part of the Project RYC2021-034006-I, funded by MICIN/AEI/10.13039/501100011033, and the European Union “NextGenerationEU”/RTRP. T.P.A. and J.T.B. acknowledge support from the Agencia Estatal de Investigación del Ministerio de Ciencia, Innovación y Universidades (MCIU/AEI) under grant “Polarimetric Inference of Magnetic Fields” and the European Regional Development Fund (ERDF) with reference PID2022-136563NB-I00/10.13039/501100011033. F.Z. acknowledges funding from the European’s Horizon 2020 research and innovation programme under grant agreement no 824135, and the Swiss National Science Foundation under grant number 200020_213147. IRSOL is supported by the Swiss Confederation (SEFRI), Canton Ticino, the city of Locarno and the local municipalities.

APPENDIX

A. THE LEVEL ENERGY OF THE MAGNETIC SUB-LEVELS AND THE MIT RATES

The level energy of the upper term $3d^5(^6S)4d^7D$ as a function of field strength shown in the left panel of Fig. A.1 are computed by diagonalizing the atomic Hamiltonian according to Eqs. (3.61a) and (3.61b) in Landi Degl’Innocenti & Landolfi (2004). The MIT rates shown in the right panel of the figure are estimated from Eq. (7.34b) in Landi Degl’Innocenti & Landolfi (2004), with $jM = j'M'$ and $j_u M_u = j'_u M'_u$. The rates corresponding to a magnetic field strength of about 3000 G are sufficiently large as to be able to neglect the contribution of the M2 transition rate, of about $2.29 \times 10^{-6} \text{ S}^{-1}$, estimated with the multi-configuration Dirac-Hartree-Fock method (Li et al. 2020). The lower term $3d^5(^6S)4p^7P^\circ$ consists of three levels with $J = 2, 3, \text{ and } 4$, respectively. The fine structure separation is on the order of 10^{-2} eV , which is much larger than the Zeeman splitting for the typical field strengths in the solar photosphere. Therefore, the level coupling is negligible, and the magnetic splitting is still linear.

REFERENCES

- Allen, C. W. 1973, *Astrophysical quantities* (London: Athlone)
- Beiersdorfer, P., Scofield, J. H., & Osterheld, A. L. 2003, *PhRvL*, 90, 235003, doi: [10.1103/PhysRevLett.90.235003](https://doi.org/10.1103/PhysRevLett.90.235003)
- Bely, O., & van Regemorter, H. 1970, *ARA&A*, 8, 329, doi: [10.1146/annurev.aa.08.090170.001553](https://doi.org/10.1146/annurev.aa.08.090170.001553)
- Brooks, D. H., Warren, H. P., & Landi, E. 2021, *ApJL*, 915, L24, doi: [10.3847/2041-8213/ac0c84](https://doi.org/10.3847/2041-8213/ac0c84)
- Chen, Y., Bai, X., Tian, H., et al. 2023a, *MNRAS*, 521, 1479, doi: [10.1093/mnras/stad583](https://doi.org/10.1093/mnras/stad583)
- Chen, Y., Li, W., Tian, H., et al. 2023b, *Research in Astronomy and Astrophysics*, 23, 022001, doi: [10.1088/1674-4527/aca8e](https://doi.org/10.1088/1674-4527/aca8e)
- . 2021a, *ApJ*, 920, 116, doi: [10.3847/1538-4357/ac1792](https://doi.org/10.3847/1538-4357/ac1792)
- Chen, Y., Liu, X., Tian, H., et al. 2021b, *ApJL*, 918, L13, doi: [10.3847/2041-8213/ac1e9a](https://doi.org/10.3847/2041-8213/ac1e9a)

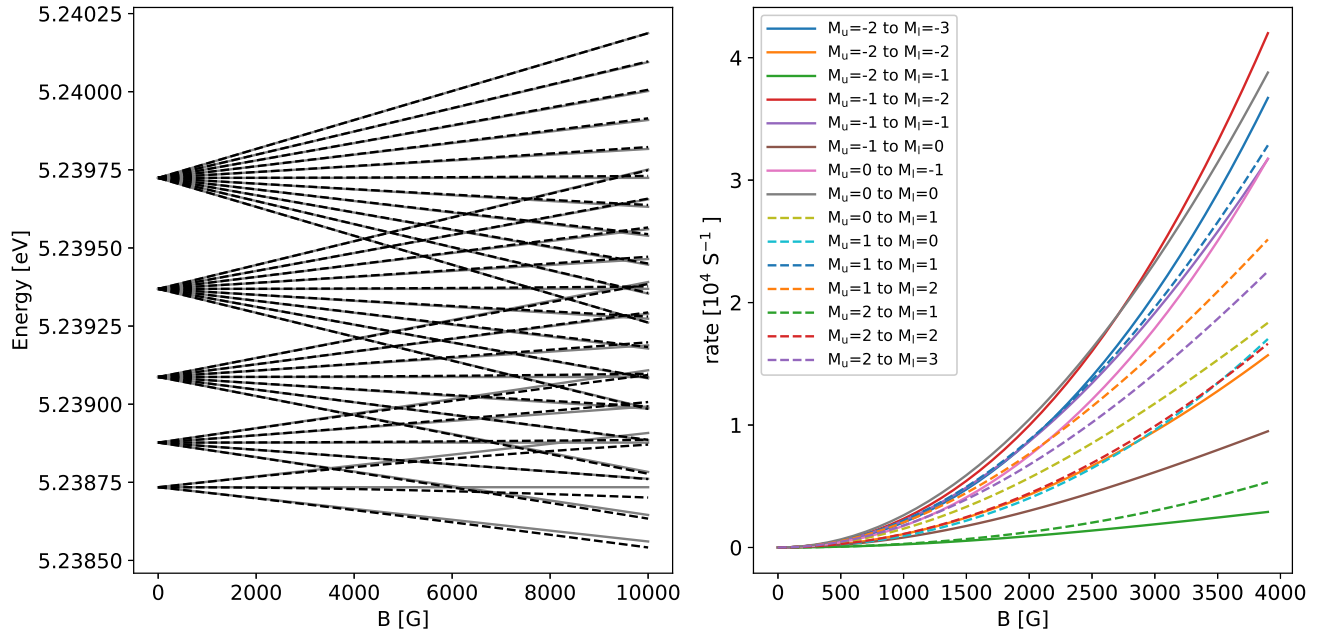


Figure A.1. Left panel: Black dashed curves show the level energy of the $3d^5(6S)4d\ ^7D$ magnetic sublevels as a function of the magnetic field strength. The gray solid curves show the same energy when assuming the linear Zeeman approximation (neglecting energy coupling). Right panel: The MIT transition rates between $3d^5(6S)4d\ ^7D_2$ and $3d^5(6S)4p\ ^7P_4^o$ states as a function of the magnetic field strength.

- Ciddor, P. E. 1996, *ApOpt*, 35, 1566, doi: [10.1364/AO.35.001566](https://doi.org/10.1364/AO.35.001566)
- Culhane, J. L., Harra, L. K., James, A. M., et al. 2007, *SoPh*, 243, 19, doi: [10.1007/s01007-007-0293-1](https://doi.org/10.1007/s01007-007-0293-1)
- del Pino Alemán, T., Casini, R., & Manso Sainz, R. 2016, *ApJL*, 830, L24, doi: [10.3847/2041-8205/830/2/L24](https://doi.org/10.3847/2041-8205/830/2/L24)
- del Pino Alemán, T., Trujillo Bueno, J., Casini, R., & Manso Sainz, R. 2020, *ApJ*, 891, 91, doi: [10.3847/1538-4357/ab6bc9](https://doi.org/10.3847/1538-4357/ab6bc9)
- Delbouille, L., Roland, G., & Neven, L. 1973, *Atlas photometrique du spectre solaire de [λ] 3000 a [λ] 10000* (Liège:Univ.deLiège,Institut d’Astrophysique)
- Fontenla, J. M., Avrett, E. H., & Loeser, R. 1993, *ApJ*, 406, 319, doi: [10.1086/172443](https://doi.org/10.1086/172443)
- Grumer, J., Brage, T., Andersson, M., et al. 2014, *PhyS*, 89, 114002, doi: [10.1088/0031-8949/89/11/114002](https://doi.org/10.1088/0031-8949/89/11/114002)
- Judge, P. G., Hutton, R., Li, W., & Brage, T. 2016, *ApJ*, 833, 185, doi: [10.3847/1538-4357/833/2/185](https://doi.org/10.3847/1538-4357/833/2/185)
- Kramida, A., Yu. Ralchenko, Reader, J., & and NIST ASD Team. 2022, NIST Atomic Spectra Database (ver. 5.10), [Online]. Available: <https://physics.nist.gov/asd> [2023, January 27]. National Institute of Standards and Technology, Gaithersburg, MD.
- Landi, E., Hutton, R., Brage, T., & Li, W. 2020, *ApJ*, 904, 87, doi: [10.3847/1538-4357/abbf54](https://doi.org/10.3847/1538-4357/abbf54)
- Landi, E., Li, W., Brage, T., & Hutton, R. 2021, *ApJ*, 913, 1, doi: [10.3847/1538-4357/abf6d1](https://doi.org/10.3847/1538-4357/abf6d1)
- Landi Degl’Innocenti, E., & Landolfi, M. 2004, *Polarization in Spectral Lines*, Vol. 307 (Dordrecht:KluwerAcademic), doi: [10.1007/978-1-4020-2415-3](https://doi.org/10.1007/978-1-4020-2415-3)
- Li, H., del Pino Alemán, T., Trujillo Bueno, J., & Casini, R. 2022, *ApJ*, 933, 145, doi: [10.3847/1538-4357/ac745c](https://doi.org/10.3847/1538-4357/ac745c)
- Li, J., Grumer, J., Li, W., et al. 2013, *PhRvA*, 88, 013416, doi: [10.1103/PhysRevA.88.013416](https://doi.org/10.1103/PhysRevA.88.013416)
- Li, W., Li, M., Wang, K., et al. 2021, *ApJ*, 913, 135, doi: [10.3847/1538-4357/abfa97](https://doi.org/10.3847/1538-4357/abfa97)
- Li, W., Grumer, J., Yang, Y., et al. 2015, *ApJ*, 807, 69, doi: [10.1088/0004-637X/807/1/69](https://doi.org/10.1088/0004-637X/807/1/69)
- Li, W., Yang, Y., Tu, B., et al. 2016, *ApJ*, 826, 219, doi: [10.3847/0004-637X/826/2/219](https://doi.org/10.3847/0004-637X/826/2/219)
- Li, W., Rynkun, P., Radžiūtė, L., et al. 2020, *A&A*, 639, A25, doi: [10.1051/0004-6361/202037794](https://doi.org/10.1051/0004-6361/202037794)
- Liu, X., Tian, H., Chen, Y., et al. 2022, *ApJ*, 938, 7, doi: [10.3847/1538-4357/ac91c7](https://doi.org/10.3847/1538-4357/ac91c7)
- Maltby, P., Avrett, E. H., Carlsson, M., et al. 1986, *ApJ*, 306, 284, doi: [10.1086/164342](https://doi.org/10.1086/164342)
- Martínez-Sykora, J., Hansteen, V. H., De Pontieu, B., & Landi, E. 2022, *ApJ*, 938, 60, doi: [10.3847/1538-4357/ac8d5b](https://doi.org/10.3847/1538-4357/ac8d5b)
- Mihalas, D. 1978, *Stellar atmospheres* (SanFrancisco:Freeman)

- Ramelli, R., Balemi, S., Bianda, M., et al. 2010, in Society of Photo-Optical Instrumentation Engineers (SPIE) Conference Series, Vol. 7735, Ground-based and Airborne Instrumentation for Astronomy III, ed. I. S. McLean, S. K. Ramsay, & H. Takami, 77351Y, doi: [10.1117/12.857120](https://doi.org/10.1117/12.857120)
- Si, R., Brage, T., Li, W., et al. 2020, ApJL, 898, L34, doi: [10.3847/2041-8213/aba18c](https://doi.org/10.3847/2041-8213/aba18c)
- van Regemorter, H. 1962, ApJ, 136, 906, doi: [10.1086/147445](https://doi.org/10.1086/147445)
- Wallace, L., Hinkle, K., & Livingston, W. C. 2005, An atlas of sunspot umbral spectra in the visible from 15,000 to 25,500 cm^{-1} (3920 to 6664 Å) (Tucson,AZ:NationalSolarObservatory)
- Xu, G., Yan, C., Lu, Q., et al. 2022, ApJ, 937, 48, doi: [10.3847/1538-4357/ac8cfa](https://doi.org/10.3847/1538-4357/ac8cfa)
- Zeuner, F., Gisler, D., Bianda, M., Ramelli, R., & Berdyugina, S. V. 2022, in Society of Photo-Optical Instrumentation Engineers (SPIE) Conference Series, Vol. 12184, Ground-based and Airborne Instrumentation for Astronomy IX, ed. C. J. Evans, J. J. Bryant, & K. Motohara, 121840T, doi: [10.1117/12.2629250](https://doi.org/10.1117/12.2629250)